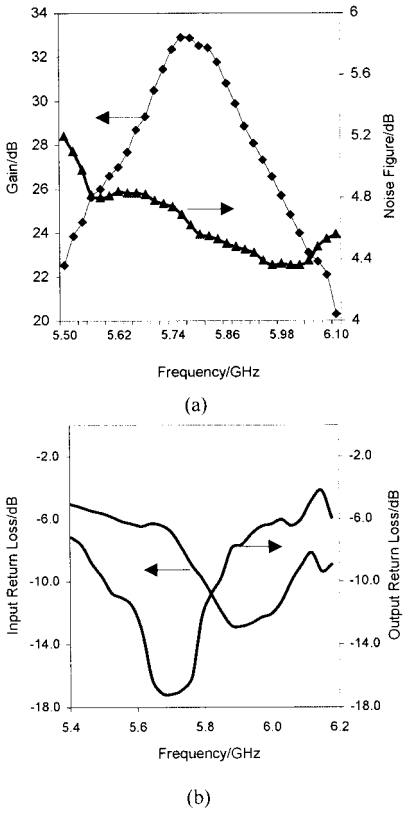

Figure 6 (a) Measured gain and noise figure; (b) return loss at the input and output ports at 3 V and 0.92 mA dc bias point

port reduces NF to 3.76 dB, which is in good agreement with the noise figure predicted without circuit losses at 5.8 GHz.

The input and output return losses measured are shown in Figure 6(b). The input return loss is −10.4 dB, and output return loss is −11.9 dB at 5.8 GHz. The input and output return losses are all less than −8 dB from 5.70 GHz to 5.9 GHz. Amplifiers with lower power consumption generally have a lower gain compression point. The designed amplifier has a measured −1-dB input compression point of −51.1 dBm, which equals to an output compression point of −19.6 dBm.

5. CONCLUSIONS

The approach and procedures utilized to design an amplifier that can simultaneously provide high-gain, low-power consumption, a low noise figure, and low return loss have been described in detail. An ultra-low-power consumption high-gain C-band silicon BJT amplifier chip has been demonstrated, using hybrid microwave integrated circuit technology. The amplifier achieves a gain-to-power-consumption ratio of 11.78 dB/mW, which is the highest benchmark in this frequency band. The high performance obtained form the amplifier under very low dc bias and low-cost HMIC fabrication technology, makes it attractive for portable RFID, ITS, and other wireless consumer applications operating in the 5.8-GHz ISM band.

ACKNOWLEDGMENTS

The authors would like to thank Weiming Tang and Ten Kwee Ng for their assistance and support during fabrication and measurement. The work is supported by the Singapore NSTB strategic research programme on MEMS.

REFERENCES

1. J. Schuermann and H. Meier, TIRIS-leader in radio frequency identification technology, Texas Instrument Tech J (1993), 2–14.
2. European prestandard on dedicated short range communication, PENV 12253, CEN/TC278, 1997.
3. H. Takenchi, A Si wide-band MMIC amplifier family for L-S band consumer product applications, 1991 IEEE MTTS Dig, 1283–1284.
4. T. Ohgihara, GaAs JFET front-end MMICs for L-band personal communications, 1993 IEEE MMICS Dig, pp. 9–12.
5. H. Monkner, A high performance 1.5 dB low noise GaAs PHEMT MMIC amplifier for low cost 1.5–8 GHz commercial applications, 1993 IEEE MMICS Dig, pp 13–16.
6. K.R. Gioffi, Monolithic L-band amplifier operation at miliwatt and sub-miliwatt DC power consumption, 1992 IEEE MMMICs Dig, pp 9–12.
7. K.W. Kobayashi and A.K. Oki, Ultra-low dc power GaAs HBT S- and C-band low noise amplifiers for portable wireless applications, IEEE Trans MTT 43 (1995), 3055–3061.
8. L. Urs, Low dc power monolithic low noise amplifier for wireless applications at 5 GHz, 1996 IEEE MMMICs Dig, pp 81–84.
9. I.A. Koullias, A 900 MHz transceiver chip set for dual-mode cellular radio mobile terminals, 1993 ISSCC Dig, pp 140–141.
10. Triquint Semiconductor, TQ9203, Low-current RFIC downconverter, Wireless Communication Products, 1995.
11. J. Engberg, Simultaneously input power match and noise optimization using feedback, 1974 European Microwave Conference, pp 385–389.

LONGITUDINAL COUPLED-CAVITY SCHEME FOR MICROWAVE-EXCITED CO_2 SLAB LASERS

A. Shahadi, Y. Sintov, and E. Jerby
Faculty of Engineering
Tel Aviv University
Ramat Aviv 69978, Israel

Received 17 July 2002

ABSTRACT: *A new microwave-excited CO_2 slab-laser scheme is demonstrated in a slow gas-flow laser experiment. The gas-discharge axial homogeneity is improved by an H-plane coupling of a rectangular resonator operating in the fundamental mode to a shorter slab laser-head resonator, below the cutoff. This paper describes the conceptual experimental and practical aspects of the microwave-excited laser.* © 2003 Wiley Periodicals, Inc. Microwave Opt Technol Lett 36: 115–120, 2003; Published online in Wiley InterScience (www.interscience.wiley.com). DOI 10.1002/mop.10692

Key words: *gas lasers; microwave excitation; discharge homogeneity*

1. INTRODUCTION

Microwave excitation of CO_2 lasers has been employed in various laser schemes since the late 1970s [1–13]. The microwave excitation is characterized by (i) availability of efficient high peak-power compact sources, (ii) alleviation of the α–γ discharge transitions due to the high-frequency discharge, and (iii) utilization of the slab configuration. The practical advantage of the microwave-excited CO_2 laser stems from the features of common microwave sources—magnetrons—which are relatively compact, low-cost, and efficient.

Fast gas-flow-, air-, or fluid-cooled cylindrical microwave-excited CO_2 lasers [1–10] enable high average laser powers. These schemes require massive pumps and heat exchangers. The in-

creased heat-dissipation rate of the slab geometry was applied in RF-excited lasers in one-channel [14–17] and multi-channel [18–23] devices, and also in compact microwave-excited lasers [11–13]. High repetition-rate pulsed microwave discharges are stabilized by a ballast dielectric strip to enable high peak and average laser powers in a stagnant gas [11].

A drawback of microwave excitation is the non-uniformity of its axial discharge due to the relatively short wavelength (as compared to RF excitation). Several methods have been proposed to improve the axial homogeneity of the microwave-excited discharge. In [2], a cylindrical laser tube was inserted into a T-shaped rectangular resonator, operated slightly above cutoff. For a symmetric microwave feeding, a cosine electric-field distribution was achieved. This technique was implemented in a tapered ridged-waveguide resonator containing a cylindrical gas tube in [10]. A TM_{010} cylindrical resonant cavity was employed in a different setup, as presented in [4]. März and Oestreicher developed a plasma source [5], in which a homogeneous discharge field was formed in a traveling-wave tapered-ridge waveguide using a resistive microwave termination. Radial microwave-discharge homogeneity in a cylindrical laser was implemented by combining orthogonal electric fields in intersecting rectangular waveguides [6]. A different approach for deriving an axial discharge uniformity was achieved by coupling a waveguide antenna to a microwave stripline, thus enabling the propagation of a TEM mode [7]. A helical excitation of a cylindrical laser was suggested as well [8, 9]. All these devices [1–10] do not employ the advantageous features of the slab configuration, and require a large overhead for gas cooling and circulation. In another design by März and Oestreicher, a double-ridged laser head was coupled in the E-plane to a varying-ridge waveguide resonator [13]. An optimized microwave coupling to the laser head was achieved by varying the dimensions of both ridged waveguides. This microwave-excited diffusion-cooled laser yielded ~0.5 W/cm^2.

Recently, an RF-excited scheme presented by Villarreal et al. [14] introduced an enhanced peak-to-average laser power ratio of 38. The laser power density-per-slab area attains ~0.8 W/cm^2. This achievement of enhanced peak-to-average power ratio marks the impressive progress of RF-excited CO_2 lasers. So far, a slab-waveguide laser head employing an axially homogeneous microwave-discharge in a uniform cross-section has not been demonstrated.

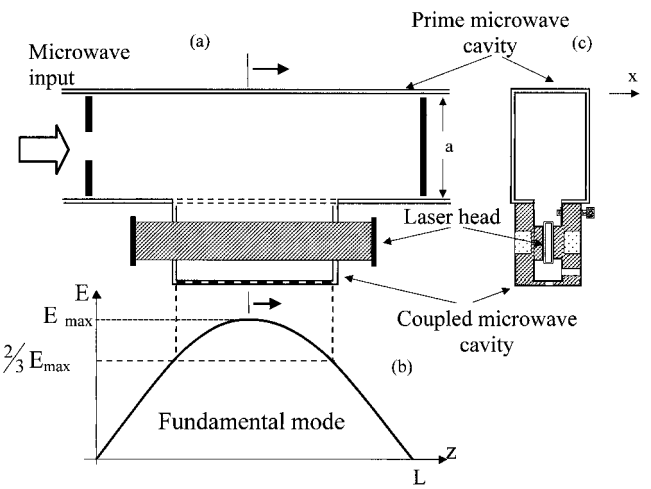

Figure 1 The coupled cavity scheme in axial (a) and transversal (c) cross-sections, and the electric field axial distribution (b)

TABLE 1 Physical Dimensions (All in Millimeters)

Rectangular Waveguide (Copper)			
Length			740
Width			61.4
Height			30.7
Double-Ridged Waveguide (Copper)			
Length			400
Width			41
Height			8
Ridge width			20
Ridges spacing			4.65
Rectangular Pyrex Tube	Corning 7740		Schott 8330
Inner height	1.5		2.0
Inner width	21.0		20.0
Wall thickness	1.5		1.3
Length		425	
Wall tolerance		±0.3	

This article presents a microwave-excitation scheme intended to obtain an axially homogeneous discharge in a slab laser with a uniform cross section. The laser excitation scheme is described in section 2. The experimental setup and results are presented in sections 3 and 4, respectively. The possible advantages of the proposed excitation scheme are summarized in section 5.

2. THE MICROWAVE EXCITATION SCHEME

The microwave-excited CO_2 slab-laser scheme is illustrated in Figure 1. The prime microwave cavity is fed by an external source through a split mirror (Fig. 1(a)). This microwave cavity is tuned to the (axial) fundamental mode by choosing a rectangular-waveguide width at almost cutoff, that is, $a \cong \lambda/2$ where λ is the microwave free-space wavelength. Therefore, the axial wavelength in this waveguide $\lambda_g = [\lambda^{-2} - (2a)^{-2}]^{-1/2}$ is "stretched" to $\lambda_g \cong 2L \gg \lambda$, where L is the cavity length (Fig. (1)). This enables the operation of the prime cavity in its fundamental (axial) mode. The coupled microwave cavity, in which the laser head is situated, is made to be shorter than the prime cavity. Hence, it is forced to oscillate below its fundamental resonance frequency. Moreover, its cross section can be widened, while it is still operated below cutoff. This cavity is coupled to the center section of the prime cavity, where the field intensity is maximal and most uniformly distributed (Fig. 1(b)), with no nulls along the discharge.

The cross section of the coupled microwave cavity (Fig. 1(c)) resembles a ridged waveguide, whereas the slab-laser head is situated in a rectangular glass tube in the ridged section. The ridged waveguide is designed to operate below cutoff. Hence, the distribution of the microwave intensity coupled into it is closely uniform. The laser tube acts as a distributed loss along the prime cavity, and the gas discharge excited in it has no zero points, although its length exceeds several wavelengths.

3. EXPERIMENTAL SETUP

The scheme presented in the previous section was implemented in a microwave-excited CO_2 slab-laser experiment. The physical dimensions of the experimental device (in millimeters) are summarized in Table 1. The microwave source is a standard 2-kW magnetron (Hitachi 2M130) at 2.45 GHz, capable of delivering 15-kW peak-power at short pulses (2–30 μs). The microwave

radiation is delivered through a circulator (Philips PDR-26) to a 60-dB coupler (Muegge MW-6971-0070) for monitoring the transmitted and reflected microwave powers. An E-H tuner provides the microwave energy matching to the prime resonator. A double-ridge waveguide is coupled sideways to the rectangular resonator by a common slit as illustrated in Figure 1. A rectangular Pyrex-tube (Table 1) is placed between the ridges, and attached to them by a silicon heat-sink compound. The tube serves as the discharge chamber, and also as the stabilizing ballast dielectric-strip required for microwave discharges. The Pyrex tube wall-thickness is designed to avoid the evolvement of thermal instabilities [24]. Two laser mirror holders are attached to the Pyrex tube by silicon microwave-proof O-rings. The gas flows through the mirror holders. Therefore, no changes are made in the standard Pyrex tube. A hemispheric optical-resonator is employed with a concave rear mirror ($R = 5$ m) and an 89% reflectivity output coupler.

A fine tuning of the discharge electric-field distribution is achieved by screws along the slit connecting the two waveguides. The laser-head is cooled by circulating water through the ridges. The average delivered microwave power is measured by a microwave-power meter (HP435A). Average heat-power discharge dissipation is measured by thermometers placed at the cooling water inlet and outlet. Average laser power is measured by an optical detector (Ophir F300A-SH).

The microwave-power homogeneity is measured by a Scalar Network Analyzer (HP8757A). This relative transmission (cold) measurement is performed in the absence of the plasma. The 2.45-GHz microwave power is injected through a coax-to-waveguide coupler, which simulates the magnetron antenna. A microwave probe inserted into a slit along the laser-head ridges couples the transmitted microwave power to the analyzer. The reflected-wave measurement (with the circulator omitted from the microwave chain) allows the input power matching.

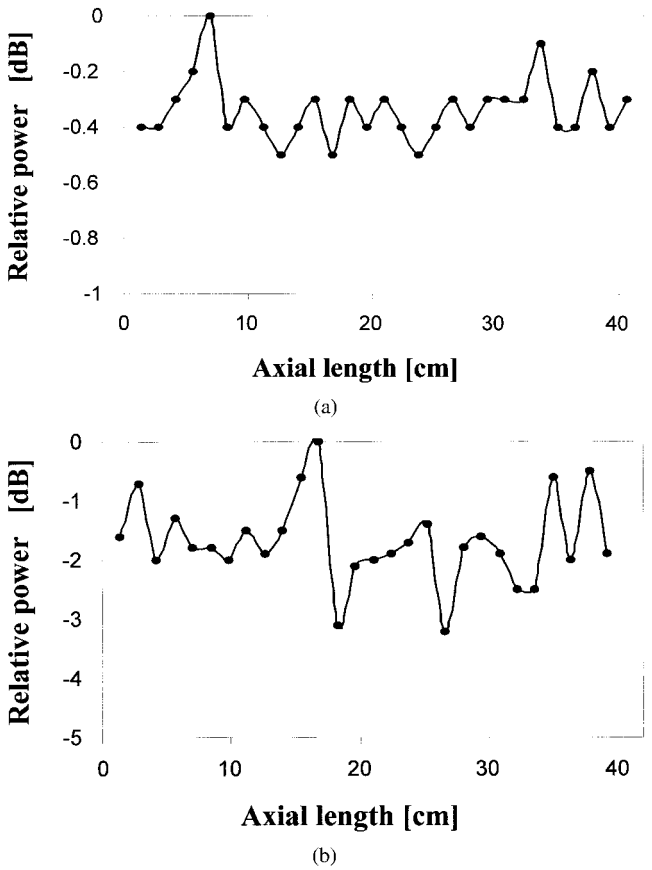

Figure 2 Microwave-power transmission measured perpendicularly beyond the ridges along the laser head, for (a) 2.0-mm and (b) 1.5-mm discharge heights

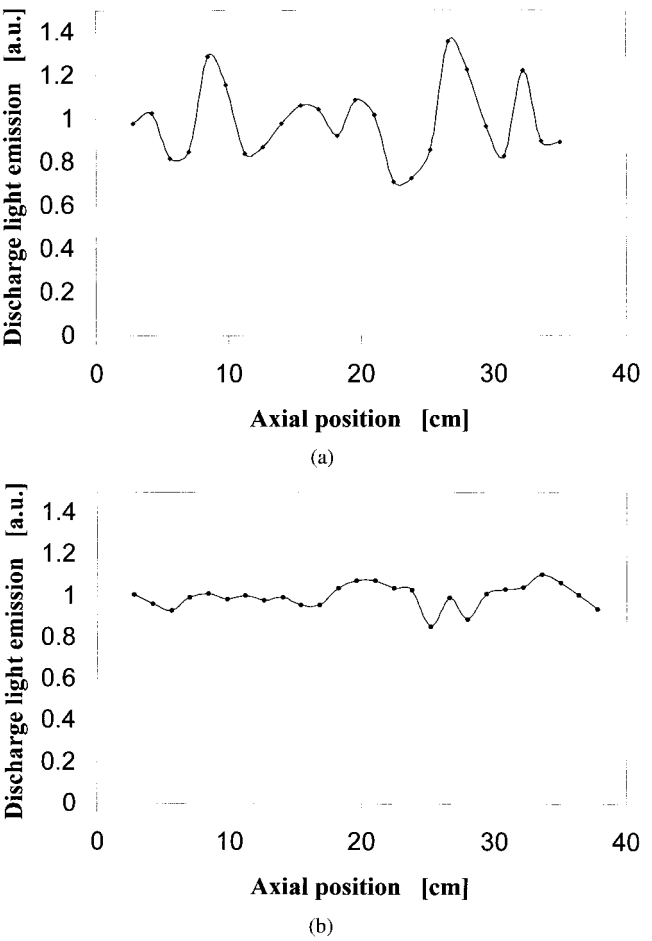

Figure 3 Distribution of the discharge light emission at 488 nm wavelength along the tube at (a) 2.0-mm and (b) 1.5-mm discharge heights

A Pyroelectric detector (Molectron P4-42) is used for the laser peak-power detection. The light-emission discharge is measured by an optical detector (Ophir PD300-3W) calibrated to a 488-nm wavelength. After setting the laser operation to its optimum by observing the output laser power, the detector is attached to each peephole along the laser head. The 5-mm-diameter peepholes are axially separated by 14 mm. The power measured at a wavelength of 488 nm indicates the rate of energy flow into the gas electronic states. The gas-flow rate did not exceed ~ 2 ℓ/s during all measurements (without the discharge), thus it can be classified as a slow-flow rate.

4. EXPERIMENTAL RESULTS

The distribution of the microwave power along the laser-head is presented in Figure 2(a) and (b), for 2.0-m and 1.5-mm discharge heights, respectively (without the laser plasma). The maximal axial deviations of the microwave power are 0.5 dB and 3.2 dB, for the 2.0-m and 1.5-mm discharge heights, respectively.

The axial homogeneity is demonstrated by the discharge light emission. The light power measured through the peepholes is presented in relative units in Figure 3(a) and (b), for the 2.0-m and 1.5-mm discharge heights, respectively. The plots show the relative light intensity along the z-axis (excluding the tube end points).

TABLE 2 Discharge Homogeneity Measurements for a $He:CO_2:N_2$ = 8:1:1 Mixture in 2.0-mm and 1.5-mm Heights

	Discharge height		
Parameter	2.0	1.5	mm
Gas pressure	95	240	Torr
Microwave pulse width	21	20	μs
Pulse repetition rate	930	1937	Hz
Ave. DC power	289	521	W
Ave. microwave power	148	340	W
Ave. laser power	6.7	15	W

Table 2 specifies the laser-operating parameters in which these homogeneity measurements are taken. The discharge light-emission variation is 17% and 5.7% (RMS), for the 2.0-m and 1.5-mm discharge heights, respectively.

The discharge light-emission power at 488 nm represents the power transferred to the gas electronic states in the discharge. The measurements presented in Figure 3(a), (b) are taken in optimal conditions regarding the output laser power. Ref. [25] presents The energy-flow rate to the gas electronic states versus the reduced field for a $He:N_2:CO_2$ = 8:1:1 mixture is presented in [25]. This data combined with the measured relative light-emission power, provides an estimate for the reduced-field variation along the tube for a near-optimum-operation condition (that is, $E/N \sim 2.5 \cdot 10^{16}$ Vcm^2). This analysis results in $\Delta E/N_{RMS} \cong 0.40 \cdot 10^{16}$ and $0.13 \cdot 10^{16}$ Vcm^2, for 2.0 and 1.5 mm discharge heights, respectively.

The total DC-to-laser power efficiency and the microwave-to-laser power efficiency versus the laser output average-power, are presented in Figure 4 (marked by (■) and (◆), respectively). The maximal efficiencies measured for the preliminary device are 12% and 9%, respectively, for both discharge heights. These efficiencies are attained at low average laser powers. Both efficiencies drop to ~5% at the maximal extracted average laser-power (40 W).

The dependence of the average and peak laser-power on the mean microwave-power is shown in Figure 5(a) and (b) and Figure 6(a) and (b), for the 2.0-m and 1.5-mm discharge heights, respectively. The maximal average and peak laser powers measured for the 2.0 mm discharge height are 35 W and 0.52 kW, respectively. For the 1.5-mm discharge height, maximal average and peak laser powers of 40 W and 0.58 kW are measured, respectively. A mixture of N_2 (18%), CO_2 (6.5%), Xe (1.5%), and He (74%), is used in this experiment.

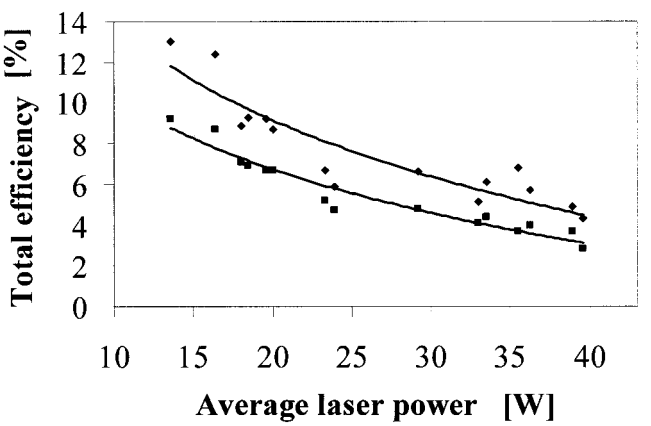

Figure 4 Total efficiency (■) and microwave-to-laser efficiency (◆) versus average laser output power

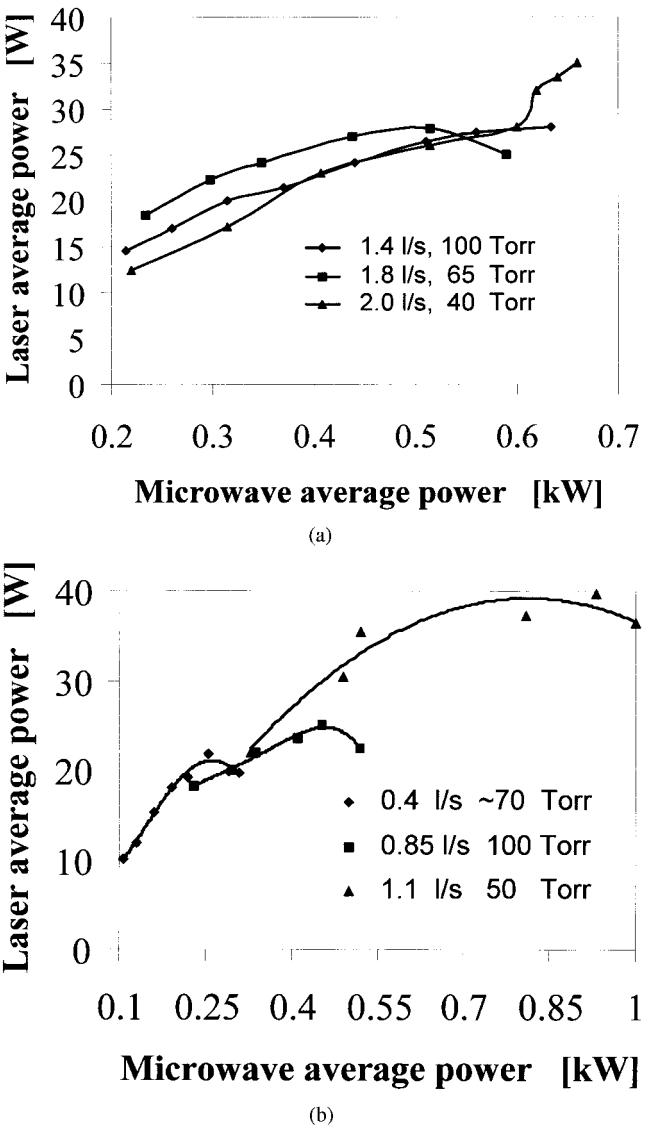

Figure 5 Average laser power versus mean inserted microwave power for different gas-flow rates at optimized gas pressures; discharge height is (a) 2.0 mm and (b) 1.5 mm

The gas flow rates and the resulting optimized gas pressures for the two discharge heights are presented in Table 3. The optimal microwave pulse-widths for the 2.0-mm and 1.5-mm discharge heights are 20–30 μs, and 10–20 μs, respectively. The pulse repetition frequency in all these measurements vary between 0.5–9.0 kHz.

5. DISCUSSION

This study demonstrates a longitudinal coupling scheme of a microwave source to a slab laser in a compact device. This design exploits the advantages of an axially homogeneous microwave discharge. The cold-waveguide transmission measurements show no field nullification along the laser head.

The homogeneity differences between the two discharge heights employed (1.5 mm and 2.0 mm) arise from the different dimensions of the Pyrex tubes used (Table 1). It should be noted that the microwave setup was basically designed for the 2.0-mm

discharge height. Thus, for the tube with a 1.5-mm discharge height, the ripple in the axial-power cold measurement is larger.

The axial variation of the reduced field (E/N) for the two discharge heights shows different axial profiles. Contrary to the cold power measurement, a lower reduced-field deviation along axis is observed for the 1.5-mm discharge height. This is due to the thicker wall of the tube with the 1.5-mm discharge height (Table 1). A thick wall represents a large impedance in series with the discharge. This impedance compensates for axial variations in the discharge electric field. Therefore, an improved axial homogeneity is observed for the 1.5-mm discharge height. Moreover, a better uniformity is possible by virtually extending the length of the rectangular waveguide-resonator beyond the laser head.

The average laser power is mainly influenced by gas temperature, degree of molecular dissociation, and discharge stability. While the laser head is designed to be thermally stable, gas heating and dissociation are proportional to the microwave pulse width and frequency. It is evident that an increased gas-flow rate results in a raise of output laser power, due to lowered dissociation of CO_2 molecules.

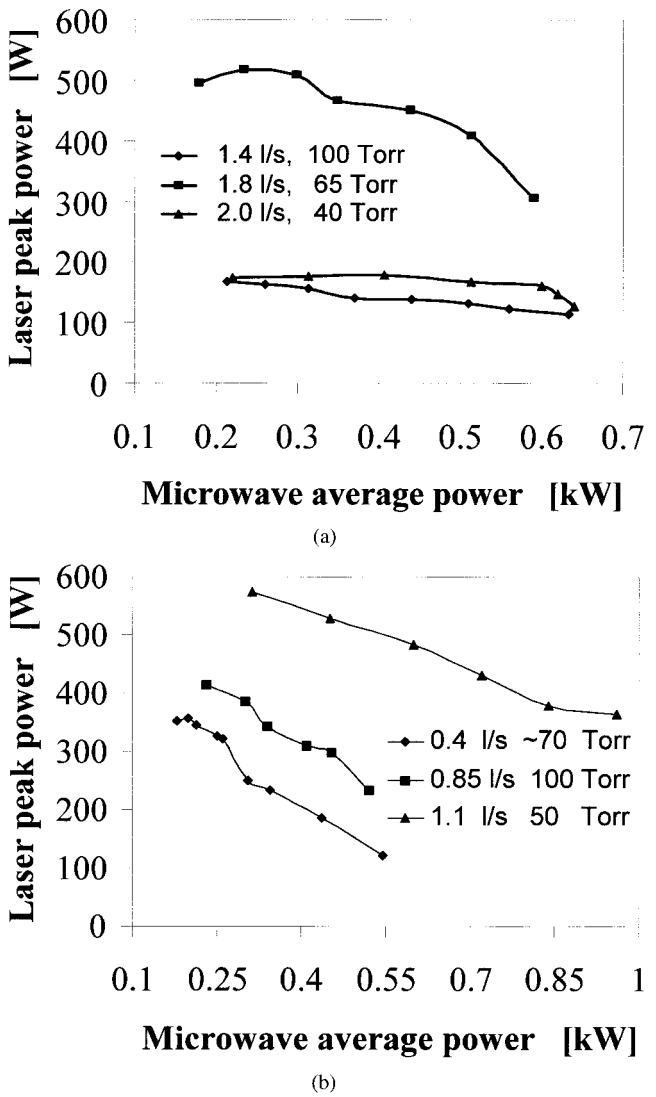

Figure 6 Peak laser power versus mean inserted microwave power for different gas-flow rates at optimized gas pressures; discharge height is (a) 2.0 mm and (b) 1.5 mm

TABLE 3 Gas Flow Rates and Optimal Gas Pressures for Two Discharge Heights

2.0-mm Discharge Height		1.5-mm Discharge Height	
Flow rate (ℓ/s)	Pressure (Torr)	Flow rate (ℓ/s)	Pressure (Torr)
1.4	100	0.4	70
1.8	65	0.85	100
2.0	40	1.1	50

The maximal pulse duration is constrained by stability considerations. However, the peak laser power is governed mainly by the maximum power delivered by the magnetron. A maximal peak power is extracted from the magnetron when its impedance is equal to that of the complex conjugate of the device input-impedance. The magnetron impedance is affected by its voltage and extracted current, its heating current, and its load-impedance. Impedance matching is achieved by an E-H tuner and screws along the laser head. Minimizing the reflected wave amplitude is used for power matching. When this is done, a maximal average microwave-power should be delivered to the laser head. Yet, the load impedance might be different from that of the magnetron. This reduces the peak microwave extracted power. Moreover, an increase in the microwave pulse frequency raises the average microwave power, but also increases the dissociation rate, resulting in lower peak laser-power and efficiency (see Fig. 4).

It should be noted that the scheme presented here might employ the benefits of forced convective cooling. A Pyrex tube with a larger aspect ratio can be inserted between the laser-head ridges with only minor design changes. Using a tube wider than the metal electrodes may enhance the transversal gas cooling effect, and therefore, increase total efficiency at high-average powers.

The experimental results for the laser operation in the slow-flow regime prove the feasibility of constructing a high-power microwave-excited CO_2 slab laser. This compact laser yields a relatively high peak-to-average power ratio. Maximum average and peak powers of 40 W and 0.58 kW, respectively, are observed.

A maximal overall efficiency of 9% is attained in our experiments at 15-W average and 305-W peak laser powers, respectively. Future designs will have to maintain this efficiency throughout the operating power regime of this laser. As compared to RF-excited slab lasers, it should be noted that the typical electro-optic efficiency of the latter attains ~10% in both sealed and slow-flow schemes for CW and pulsed operation [14]. This efficiency level is not much higher than that obtained by the microwave-excited slow-flow CO_2 laser experiment presented in this paper.

The major objective of this study, to develop a microwave-excited laser CO_2 slab-laser scheme characterized by an axially homogeneous discharge, was accomplished as presented in this paper. This may lead to the development of more efficient high-power compact CO_2 lasers utilizing the known practical advantages of the magnetron as a microwave source.

REFERENCES

1. O.S. Vasutinskii, V.A. Kruzhalov, T.M. Perchanok, D.K. Terekhin, and S.A. Fridrikhov, Pulsed microwave discharge as a pump for the CO_2 laser, Sov Phys Tech Phys 23 (1978), 189–194.
2. B. Freisinger, H. Frowein, M. Pauls, G. Pott, J.H. Schäfer, and J. Uhlenbusch, Excitation of CO_2 lasers by microwave discharges, SPIE, CO_2 Lasers Applic II 1276 (1990), 29–40.
3. R. Wester and S. Seiwert, Investigation of microwave excited CO_2 laser discharges, J Phys D: Appl Phys 24 (1991), 1102–1107.

4. T. Ikeda, M. Danno, H. Shimazutsu, T. Abe, and J. Tanaka, TM_{010}-mode microwave excited high power CO_2 laser using a cylindrical resonant cavity, IEEE J Quantum Electr 30 (1994), 2657–2662.
5. M. März and W. Oestreicher, A versatile microwave plasma source and its application for a CO_2 laser, Rev Sci Instr 65 (1994), 2980–2983.
6. M. Kato, K. Saito, H. Yagima, K. Sato, M. Kimura, N. Furuya, S. Yamane, Microwave-discharge-excited CO_2 laser using orthogonally crossing electric fields, National-Technical-Report 43 (1997), 26–33.
7. N. Matsuoka, T. Tokoro, M. Yasuda, and T. Uchiyama, CO_2 laser excited by microwave discharge using stripline, Rev-Laser-Eng 25 (1997), 67–61.
8. P.J. Dobie, J.A. Broadhead, and A. Maitland, Microwave excitation of lasers using TWT helices, ITG Fachberichte 108 (1989), 347–351.
9. T. Ikeda, M. Danno, T. Monaka, M. Noda, and J. Tanaka, A new helical coupling microwave antenna excited high-power CO_2 laser using cylindrical resonant cavity, IEEE J Quantum Electr 35 (1999), 721–729.
10. M.W. Murray, K.M. Dickenson, United States Patent, Number US5684821A, November, 1997.
11. Y. Sintov, A. Gabay, S. Yatsiv, Self-activated, forced convective cooling in a pulse slab CO_2 laser, J Phys D: Appl Phys 30 (1997), 2530–2535.
12. J. Nishime and K. Yoshizawa, Development of CO_2 laser excited by 2.45 GHz microwave source, SPIE, High-Power Gas Lasers 1225 (1990), 340–348.
13. M. März and W. Oestreicher, Microwave excitation of a diffusion-cooled CO_2 laser, J Phys D: Appl Phys 27 (1994), 470–474.
14. F. Villareal, P.R. Murray, H.J. Baker, and D.R. Hall, Enhanced peak power and short pulse operation of planar waveguide CO_2 lasers, Appl Phys Lett 78 (2001), 2276–2278.
15. S. Yatsiv, Conductively cooled capacitively coupled RF excited CO_2 lasers, Gas Flow and Chemical Lasers, Proceeding of the 6th International Symposium (1986), 252–257.
16. S.V. Kukhlevskii, A.S. Provorov, and M. Yu. Reushev, Waveguide laser utilizing the sequence bands obtained by transverse rf excitation through a dielectric, Sov J Quantum Electr 19 (1989), 308–310.
17. A.I. Dutov, I. Yu. Evstratov, V.N. Ivanova, A.A. Kuleshov, S.A. Motovilov, N.A. Novoselov, V.E. Semenov, V.N. Sokolov, M.S. Yur'ev, Experimental investigation and numerical simulation of a slab waveguide CO_2 laser with rf pumping, Kvatovaya Elektronika 23 (1996), 499–503.
18. A. Lapucci and G. Cangioli, Triple slab radio-frequency discharged CO_2 laser, Appl Phys Lett 62 (1993), 7–9.
19. A.M. Hornby, H.J. Baker, D.R. Hall, Combined array/slab waveguide CO_2 lasers, Opt Commun 108 (1994), 97–103.
20. S.J. Scalise, D.W. Davis, United States Patent, Number US5475703, December, 1995.
21. K.M. Abramski, A.D. Colley, H.J. Baker, and D.R. Hall, High-power two-dimensional waveguide CO_2 laser arrays, IEEE J Quant Electr 32 (1996), 340–349.
22. J.D. Strohschein, W.D. Bilida, H.J.J. Seguin, and C.E. Capjack, Enhancing discharge uniformity in a multi-kilowatt radio frequency excited CO_2 slab laser array, Appl Phys Lett 68 (1996), 1043–1045.
23. W.D. Billida, H.J.J. Seguin, and C.E. Capjack, Grid separation oscillator using resonant coaxial cavities for high power multichannel laser, Rev Sci Instr 67 (1996), 4045–4049.
24. Y. Sintov and A. Shahadi, Thermal-instability considerations for pulsed microwave-excited CO_2 slab-lasers, J Phys D: Appl Phys 33 (2000), 2125–2132.
25. T. Ledig and B. Schroder, Electron energy distribution function and power transfer data for radio-frequency discharges in CO_2 laser gas mixtures, J Phys D: Appl Phys 23 (1990), 1624–1632.

ANALYSIS OF A BILATERAL DISTRIBUTED AMPLIFIER USING SCATTERING PARAMETERS

Mehdi Si Moussa, Mohamed Trabelsi, and Rabia Aksas
Electrical Engineering Department
Ecole Nationale Polytechnique
10 Avenue Hassan badi, B.P. 182 El-Harrach
Algiers 16200, Algeria

Received 12 July 2002

ABSTRACT: *A formulation for the bilateral distributed amplifier network using a normalized transmission matrix approach is proposed in this letter. The analysis takes into consideration the effect of C_{gd} in the active device. Our approach is compared to the theoretical predictions for the unilateral case and measured results.* © 2003 Wiley Periodicals, Inc. Microwave Opt Technol Lett 36: 120–122, 2003; Published online in Wiley InterScience (www.interscience.wiley.com). DOI 10.1002/mop.10693

Key words: *bilateral distributed amplifier; scattering parameters; normalized transmission matrix*

1. INTRODUCTION

For over a decade, the distributed amplifier has been one of the topologies especially suited for wideband amplification, due to its moderate gain and noise figure [1–3]. In this paper, we propose to extend the normalized-transmission matrix formalism to a bilateral-distributed amplifier. The proposed method takes into account the effect of feedback due to the MESFET's gate-drain capacitance and its influence on the behavior of the distributed amplifier.

2. THEORY

The normalized-transmission matrix approach was presented by McKay et al. [4]. This theory applies to a general class of distributed amplifier (see Fig. 1) with discrete sampling points on the gate line, which couple to discrete excitation points on the drain line. This paper extends this concept by considering the bilateral case obtained by including the gate-drain capacitance C_{gd} of the MESFET. Using the scattering formalism, the wave quantities as shown in Fig. 2 are given by

$$b_n^{\pm} = \frac{V_{b_n}}{\sqrt{Z_{0_d}}} \pm i_{b_n}\sqrt{Z_{0_d}} \tag{1}$$

$$a_n^{\pm} = \frac{V_{a_n}}{\sqrt{Z_{0_g}}} \pm i_{a_n}\sqrt{Z_{0_g}} \tag{2}$$

$$a_n'^{-} = (a_n^{-} + a_{n+1}^{+}) - \frac{a_n^{+} + a_n^{-}}{2}, \tag{3}$$

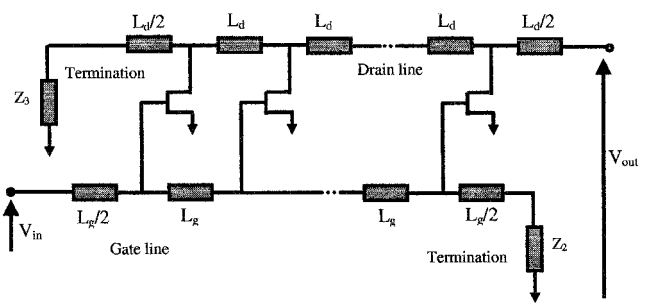

Figure 1 Schematic representation of a distributed amplifier